AAPS PharmSciTech **2003; 4 (2) Article 22 (http://www.pharmscitech.org).**

Simulating the Hydrodynamic Conditions in the United States Pharmacopeia Paddle Dissolution Apparatus

Submitted: February 11, 2003; Accepted: March 31, 2003

Leonard G. McCarthy[1], Carolin Kosiol[2], Anne Marie Healy[1], Geoff Bradley[2], James C. Sexton[2], and Owen I. Corrigan[1]

[1]Department of Pharmaceutics and Pharmaceutical Technology, Trinity College Dublin, Ireland
[2]Department of Mathematics and Trinity Centre for High Performance Computing, Trinity College Dublin, Ireland

ABSTRACT

The objective of this work was to examine the feasibility of developing a high-performance computing software system to simulate the United States Pharmacopeia (USP) dissolution apparatus 2 (paddle apparatus) and thus aid in characterizing the fluid hydrodynamics in the method. The USP apparatus was modeled using the hydrodynamic package Fluent. The Gambit program was used to create a "wireframe" of the apparatus and generate the 3-dimensional grids for the computational fluid dynamics solver. The Fluent solver was run on an IBM RS/6000 SP distributed memory parallel processor system, using 8 processors. Configurations with and without a tablet present were developed and examined. Simulations for a liquid-filled vessel at a paddle speed of 50 rpm were generated. Large variations in fluid velocity magnitudes with position in the vessel were evident. Fluid velocity predictions were in good agreement with those previously published, using laser Doppler velocity measurements. A low-velocity domain was evident directly below the center of the rotating paddle. The model was extended to simulate the impact of the presence of a cylindrical tablet in the base of the dissolution vessel. The presence of the tablet complicated the local fluid flow, and large fluid shear rates were evident at the base of the compact. Fluid shear rates varied depending on the tablet surface and the location on the surface and were consistent with the reported asymmetrical dissolution of model tablets. The approach has the potential to explain the variable dissolution results reported and to aid in the design/prediction of optimal dissolution conditions for in vitro–in vivo correlations.

Corresponding Author: Anne Marie Healy, Department of Pharmaceutics and Pharmaceutical Technology, Trinity College Dublin, Ireland. Phone: +353-1-6081444; Fax: +353-1-6082783; Email: healyam@tcd.ie.

KEYWORDS: computational fluid dynamics (CFD), USP paddle apparatus, dissolution, hydrodynamics, modeling

INTRODUCTION

Appropriate dissolution medium hydrodynamics are necessary to optimize the likelihood of successfully developing good in vitro–in vivo correlations (IVIVCs),[1-3] particularly for immediate release products. In situations where dissolution is the rate-determining step controlling absorption, the fluid hydrodynamics will influence the dissolution rate and hence the rate of absorption. Therefore, in the development of IVIVCs, it is important that in vitro dissolution conditions correspond to those experienced in vivo. While the United States Pharmacopeia (USP) paddle apparatus (apparatus 2)[4] is the most widely used dissolution method, despite its simple design, the hydrodynamics are complex and not well understood. Recently, different intrinsic dissolution rates from different surfaces of a nondisintegrating compact were measured, reflecting the complex hydrodynamics of the system.[5]

The objective of this work was to examine the feasibility of developing a high-performance computing software system to simulate the USP dissolution apparatus 2 and thus aid in characterizing the fluid hydrodynamics. Such a system would be useful in the evaluation of the effect of apparatus modifications on fluid flow and dissolution.

Relatively mild agitation conditions are considered to be present in the gastrointestinal tract.[1,6,7] Thus, x-ray and gastroscopic studies have shown that on ingestion, following disintegration of a rapidly disintegrating formulation, particles do not immediately disperse throughout the stomach but rather remain as an aggregate,[1] for up to 50 minutes in some cases.[8] Thus, it is the overall surface area of this aggregate or "mound"

that dictates the dissolution rate. Levy[1] studied plain and buffered acetylsalicylic acid (ASA) tablets and found that at high agitation intensities no differences in dissolution were evident between the 2 formulations; however, when a paddle-type apparatus, the "beaker method," that employed slow agitation conditions and permitted aggregate/"mound" formation following disintegration was used, the buffered tablets dissolved more rapidly, consistent with the results of an in vivo bioavailability study. A further study, performed in the same beaker apparatus using 3 different dosage forms of ASA exhibiting very different absorption characteristics and an agitation rate of 60 rpm, failed to correlate with in vivo absorption data. However, when the dissolution data were obtained at 50 rpm, a satisfactory correlation was obtained, encompassing all 3 products.[9] Luminal hydrodynamics were also recently shown to be an important factor in the absorption rate of felodipine from course suspensions in dogs.[10] Thus, in establishing IVIVCs, the hydrodynamic conditions are critical.

Experimental measurements of fluid velocities in the USP paddle dissolution apparatus have been previously undertaken,[11,12] but laser Doppler measurements give results for single points in space only. Bulk fluid flow between these points is then speculated based on the results obtained. The application of computational fluid dynamics (CFD) to determine the hydrodynamics throughout the vessel of the USP paddle dissolution apparatus is a novel approach to examining this problem.

MATERIALS AND METHODS

Use of the Fluent CFD Package

Modeling the USP Apparatus with No Tablet Present

The USP apparatus was modeled using the CFD package Fluent version 5.4.8 (Fluent Incorporated, Canterra Resource Park, NH). Fluent is a state-of-the-art computer program for modeling fluid flow and heat transfer in complex geometries.[13]

CFD involves the numerical solution, by computational methods, of the governing equations that describe fluid flow. These are the continuity equation (conservation of mass) (eg, Equation 1, for cylindrical coordinates[14]), the set of the Navier-Stokes equations (conservation of momentum) (eg, Equation 2, 3 and 4, for cylindrical coordinates[14]), and any additional conservation equations, for example, energy (for nonisothermal systems) or species concentrations.

$$\frac{\partial \rho}{\partial t} + \frac{1}{r}\frac{\partial (r\rho v_r)}{\partial r} + \frac{1}{r}\frac{\partial (\rho v_\theta)}{\partial \theta} + \frac{\partial (\rho v_z)}{\partial z} = 0 \quad (1)$$

$$\rho\left(\frac{\partial v_r}{\partial t} + v_r\frac{\partial v_r}{\partial r} + \frac{v_\theta}{r}\frac{\partial v_r}{\partial \theta} - \frac{{v_\theta}^2}{r} + v_z\frac{\partial v_r}{\partial z}\right) = -\frac{\partial p}{\partial r} + \rho g_r + \mu\left(\frac{1}{r}\frac{\partial}{\partial r}\left(r\frac{\partial v_r}{\partial r}\right) - \frac{v_r}{r^2} + \frac{1}{r^2}\frac{\partial^2 v_r}{\partial \theta^2} - \frac{2}{r^2}\frac{\partial v_\theta}{\partial \theta} + \frac{\partial^2 v_r}{\partial z^2}\right) \quad (2)$$

$$\rho\left(\frac{\partial v_\theta}{\partial t} + v_r\frac{\partial v_\theta}{\partial r} + \frac{v_\theta}{r}\frac{\partial v_\theta}{\partial \theta} + \frac{v_r v_\theta}{r} + v_z\frac{\partial v_\theta}{\partial z}\right) = -\frac{1}{r}\frac{\partial p}{\partial \theta} + \rho g_\theta + \mu\left(\frac{1}{r}\frac{\partial}{\partial r}\left(r\frac{\partial v_\theta}{\partial r}\right) - \frac{v_\theta}{r^2} + \frac{1}{r^2}\frac{\partial^2 v_\theta}{\partial \theta^2} + \frac{2}{r^2}\frac{\partial v_r}{\partial \theta} + \frac{\partial^2 v_\theta}{\partial z^2}\right) \quad (3)$$

$$\rho\left(\frac{\partial v_z}{\partial t} + v_r\frac{\partial v_z}{\partial r} + \frac{v_\theta}{r}\frac{\partial v_z}{\partial \theta} + v_z\frac{\partial v_z}{\partial z}\right) = -\frac{\partial p}{\partial z} + \rho g_z + \mu\left(\frac{1}{r}\frac{\partial}{\partial r}\left(r\frac{\partial v_z}{\partial r}\right) + \frac{1}{r^2}\frac{\partial^2 v_z}{\partial \theta^2} + \frac{\partial^2 v_z}{\partial z^2}\right) \quad (4)$$

The components of velocity are given by $v = v_r, v_\theta, v_z$, where v_r is the radial component of velocity, v_θ is the tangential component of velocity, and v_z is the axial component of velocity. r is distance in the radial direction, θ is distance in the tangential direction, and z is distance in the axial direction. p is pressure, μ is dynamic viscosity, and ρ is density of the fluid. g_r, g_θ, and g_z are the components of the acceleration of gravity vector in the radial, tangential, and axial directions, respectively.

The CFD analysis begins with the construction of the geometry of the system or domain to be analyzed. This domain is then subdivided into small volumes (or cells) by a meshing process and the governing equations of fluid flow are then solved for each cell within the mesh.

The problem is split into 2 main sections, grid formation and solver execution. The CFD package contains a series of tools, the 2 core programs being Gambit and Fluent. Gambit is the preprocessor, which is used to generate the computational domain, to perform geometry modeling, and to develop the initial grid or mesh. This produces a file called a "mesh file," which is the connector file between the preprocessor and the solver (the Fluent program). Once the grid has been read into the solver, all remaining operations are performed within it. These include setting boundary conditions, defining fluid properties, executing the solution, refining the grid, and viewing and postprocessing the results.

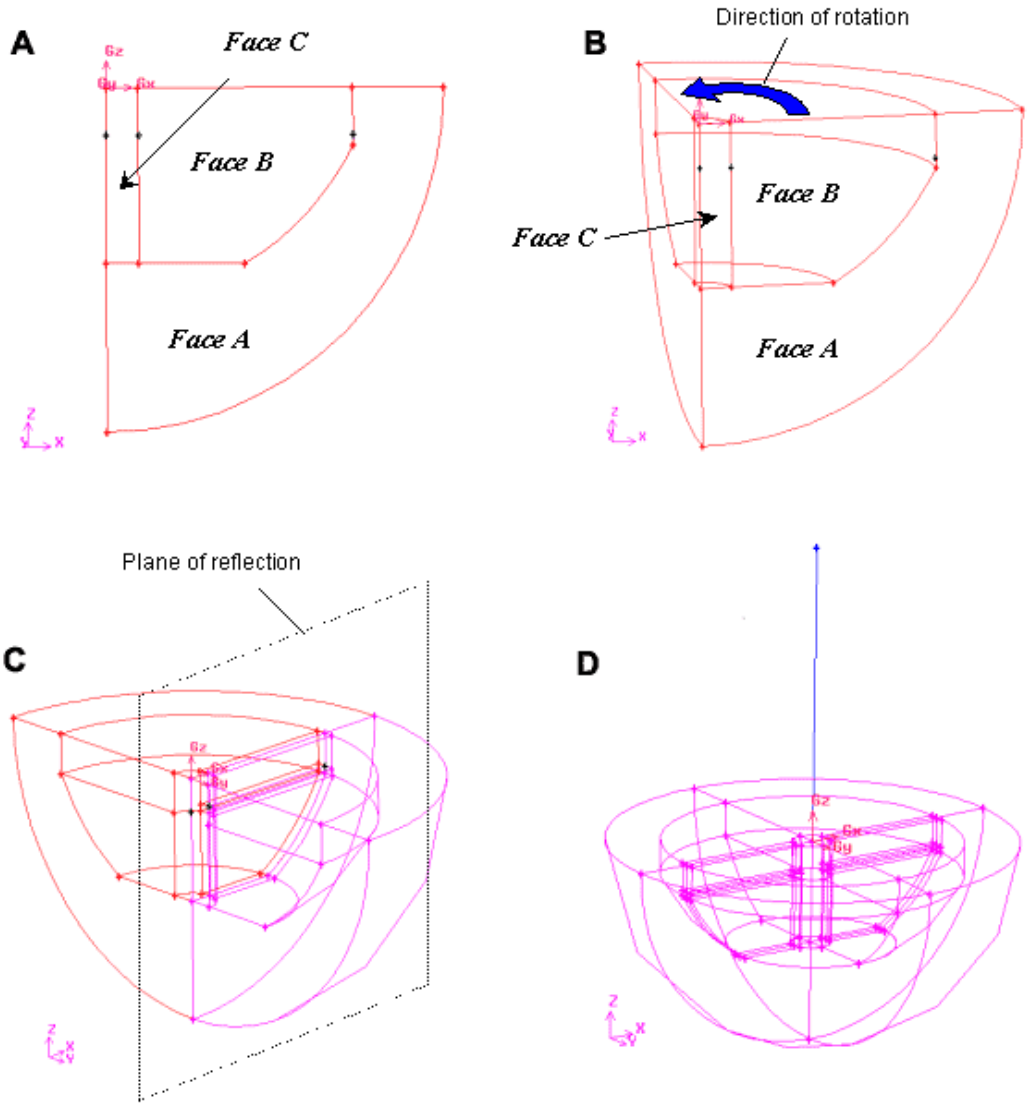

Figure 1. GAMBIT graphical interface diagram illustrating some of the steps involved in the generation of a quarter of the vessel hemisphere and the lower section of the paddle: (A) creation of 2-dimensional edges of stirrer and hemisphere, (B) formation of quarter-hemispherical volume after rotation of 2-dimensional edges, (C) use of reflection plane to produce half of hemispherical bottom, and (D) creation of "sweep" edge prior to extrusion of cylindrical volume.

Creation of the Dissolution Vessel

A wireframe geometry of the USP vessel was built up in the preprocessor, initially from 2-dimensional sections, which were manipulated into 3-dimensional sections that would eventually compose the overall volume of the USP paddle apparatus. The hemispherical bottom of the vessel consisted of 4 quarter-hemispheres that were formed by reflection from an initial quarter. This initial quarter was built from a bottom-up approach of vertex to edge to face to volume progression.

The important vertices of a plane, midway through the paddle wings, were individually defined using 3-dimensional coordinates, based on the USP compendial specifications. Individual edges of the paddle and vessel geometry, both straight and curved, were formed using the relevant vertices. The individual edges were then merged to define faces A, B, and C (**Figure 1A**). Faces A, B, and C were rotated 90° about an axis defined as the center of the paddle shaft, producing a quarter-hemispherical volume that contained the main geometrical features of the paddle and vessel hemisphere (**Figure 1B**). Three volumes were then defined,

by merging the relevant faces. A plane of reflection was set up that allowed the production of half of the hemispherical section of the apparatus, via reflection in this plane (**Figure 1C**). The introduction of another plane of reflection at this stage completed the full geometry of the lower hemisphere of the apparatus, including the paddle and wings.

A vertex was introduced corresponding to the center point of the paddle shaft at the level of the top of the dissolution medium volume. A virtual "sweep edge" was then introduced by connecting this vertex with the center point of the vessel hemispherical bottom (**Figure 1D**). The 16 faces of the top surface of the hemispherical bottom were selected and "swept" in the direction of the virtual edge. This extrusion of faces produced 16 new volumes corresponding to the upper cylindrical volume of the apparatus and the upper portion of the paddle shaft.

Introduction of Meshing Boundary Layers

The steep gradients in velocity and pressure involved in the regions of interface between fluid and solid components can complicate solution convergence. One tool to combat this problem is the ability to introduce meshing "boundary layers" in the fluid at any fluid-solid interface. This feature allows the user to define the thickness of the first layer of grid cells at the interface, the ratio of the thickness of subsequent layers, and the total number of boundary layers at the interface. This tool was used to apply meshing boundary layers at all interfaces between solid and fluid on the vessel volume. The criteria used for the formation of the boundary layers are shown in **Table 1**.

Table 1. Criteria Used for the Formation of the Meshing Boundary Layers (Without Inclusion of Compact)

Solver Formulation Input	Setting
First layer	200 μm
Growth factor	1.5
Total depth	1.63 mm
Number of rows	4
Internal continuity	No
Corner shape	Block
Transition pattern	1:1
Transition rows	0

Mesh Generation

A structured hexahedral mesh was used. The wireframe of the dissolution apparatus that was generated consisted of a large number of individual volumes that were meshed individually into hexahedral cell units.

The 3-dimensional hexahedral mesh setup was developed by refinement of individual sections of the grid in regions of high-velocity gradient by a gradual development process of successive grids to arrive at the final setup. The examined grids contained between 500 000 and 2 000 000 individual cells.

The vessel fluid volume was defined as a rotating reference frame with angular rotation of 5.236 rad/s (50 rpm), while the stirrer wall was stationary in the absolute reference frame. The vessel wall was defined as a rotating wall with an angular rotation of 0 rad/s (stationary in the absolute frame). "Water-liquid" with a predefined viscosity (1.003×10^{-3} kg/m.s) at room temperature (20°C) was chosen as the material for the vessel volume.

It was desirable to have an area of high mesh refinement in the region of the stirrer wings. A region of very high refinement was produced in the cells immediately beside the paddle by using the "hanging node" adaptation process. Each cell within a distance of 4 cells from the paddle surface was divided isotropically from a hexahedron into 8 hexahedra.

Grid Partitioning and Parallelization

Parallel processing on a multiprocessor system with the CFD program involved partitioning of the grid into a number of parts using the serial solver, initiation of the parallel solver, reading of the partitioned case file, and calculation of the solution. All calculations were on an IBM RS/6000 SP processor system using 8 processors. Therefore, the complete domain was divided into 8 subdomains, using "cylindrical Z axis" as the bisection method.

The CFD solver solves the governing integral equations for the conservation of mass and momentum numerically. Because there are 3 momentum equations involved in a 3-dimensional problem, there are 4 residuals of error (momentum in 3 directions and the continuity equation) to be monitored for convergence, the point at which the solution is deemed to be complete. Convergence criteria of $1e^{-3}$ were used.

Introduction of a Cylindrical Tablet to the Vessel

A cylinder of 13 mm diameter with a height of 8.5 mm was set up at the base of the vessel. This cylindrical volume was then "intersected" with the 4 quarters of the hemispherical base of the dissolution vessel to define the new fluid volume of the vessel.

Following the introduction of the compact, the setup in the preprocessor was the same as that described above, with regard to meshing boundary layer inclusion, mesh generation using the hexahedral approach, and boundary and continuum setup. In this case, however, a user-defined liquid was input as the material for the vessel volume. This allowed the viscosity of the liquid to be set to that of water at 37°C (0.6943×10^{-3} kg/m.s).[15] The inclusion of the compact complicated the meshing process in the hemispherical region of the vessel. Meshing was facilitated by ensuring that individual edges of the top circular face quarters of the compact were meshed in exactly the same manner as the bottom circular face quarters of the paddle.

Comparison with Laser Doppler Measurements to Validate CFD Simulations

To validate the CFD solution to fluid flow in the dissolution apparatus, simulated velocities, generated using the CFD approach, were compared with experimental measurements reported by Bocanegra et al.[11] The latter authors produced laser Doppler measured velocity profiles from a series of planes at various heights and radii within the USP paddle apparatus, with outputs of axial, radial, and tangential velocities as illustrated by **Figure 2**.

The velocity profiles produced consisted of normalized velocity components for different radii at a certain plane height versus "paddle relative position in degrees" (ie, the angle made between the point in the vessel being analyzed and the position of the paddle). All the velocity data were normalized to the paddle tip speed (0.196 m/s at 50 rpm). Geometrical parameters were also normalized. The height of the fluid level (75.5 mm) measured from the plane where the hemispherical bottom develops and the radius of the hemispherical bottom (51 mm), respectively, are used in the normalization process. The normalized coordinate system adopted by Bocanegra et al[11] is indicated in **Figure 3**.

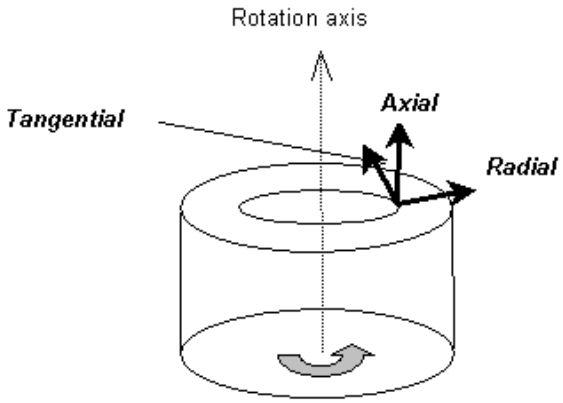

Figure 2. Cylindrical velocity components. In the paddle apparatus, positive axial indicates motion toward the liquid surface, positive radial indicates motion toward the wall, and positive tangential indicates motion in the direction of paddle rotation.

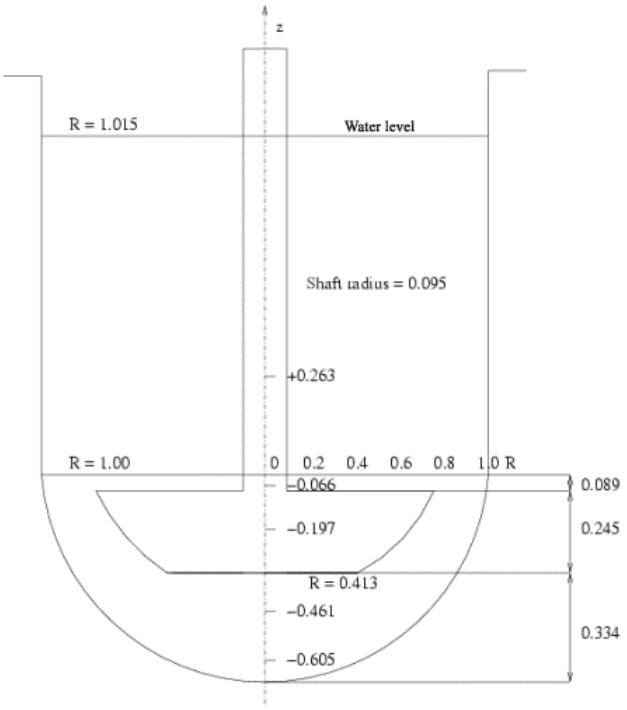

Figure 3. Normalized coordinate system used by Bocanegra et al[11] for the USP dissolution apparatus, where $R = r/r_w$ (r_w = 50.8 mm, the radius of the vessel above the hemispherical base) and $Z = z/z_1$ (z_1 = 75.5 mm, the height of the dissolution medium from the center of the hemispherical base). The horizontal planes—Z = 0.263, Z = –0.066, Z = –0.197, Z = –0.461, and Z = –0.605—represent the horizontal heights of virtual planes in the vessel, where fluid velocity measurements were made.

RESULTS AND DISCUSSION

The fluid velocities, midplane in line with the paddle wings (**Figure 4A**) and at 90° to the paddle wings (**Figure 4B**), simulated at 50 rpm are shown in **Figure 4**. Large variations in fluid velocity vectors with position in the vessel were evident, particularly in the vicinity of the paddle tips (**Figure 4**). A low-velocity domain was evident directly below the center of the rotating paddle (**Figure 4**). Comparison of **Figures 4A** and **4B** indicates significant differences in velocity vector magnitude/intensity in some regions but not in others, depending on the relative stage of rotation of the paddle.

The CFD technique used (grid setup and solver approach) was validated by comparing simulated velocity outputs with experimental data generated by Bocanegra et al[11] using laser Doppler velocity measurements. CFD-generated tangential, axial, and radial velocities were compared with the published data of Bocanegra et al[11] using the normalized (dimensionless) coordinate system outlined by these authors. While laser Doppler measurements can provide only a single point in space measurement of any component of fluid velocity for each experimental determination, CFD can predict velocity measurements, simultaneously, for each node in the computational domain (effectively for hundreds of thousands to millions of points in the vessel).

Tangential Velocities 2 mm (Z = –0.066) Above the Paddle

Among the more variable hydrodynamic regions in the USP 2 dissolution method is a plane just above the rotating paddle, such as Z = –0.066 (see **Figure 3**) —that is, 2.0 mm above the paddle. The normalized (relative to the paddle tip) measured (Bocanegra et al[11]) and predicted (CFD) tangential velocities versus paddle angle are shown in **Figures 5A** and **5B**. It is seen, in both sets of data, that a 180° periodic tangential velocity exists, reflecting the 2-blade nature of the paddle. Velocities decrease as the paddle approaches the measuring volume (paddle relative positions of 0° and 180°) and then increase. The velocities tend to increase, and become more variable, with increasing radius until beyond the paddle tip, when they decrease. These radius-related changes are more pronounced in the CFD data.

Tangential Velocities 5.3 mm (Z = –0.605) from the Base of the Vessel

In contrast to velocities in the region just above the paddle, velocities close to the bottom of the vessel are much less variable with paddle rotation position, and they increase consistently with radius. The normalized (relative to paddle tip) predicted tangential velocities (at the appropriate Bocanegra radii[11]) are shown in **Figure 6**. Qualitatively, experimental results and simulated results compare favorably. A flat profile over all angles is exhibited for both results, indicating that there is no periodicity with regard to tangential velocities toward the base of the vessel (except for some minor curvature with the lowest radius for the simulated results). Quantitatively, the results also compare well. The lowest radius simulated results vary between 0.1 and 0.2, while the experimental values center around 0.15. The next radius ranges from 0.2 to 0.3, with an experimental mean of approximately 0.25. Similarly, tangential velocities at the third and fourth radii are in the region of around 0.35 and 0.45, respectively, comparing very well with the experimental values. It is possible to convert angular rotation of the paddle to tangential velocities at various radii of the paddle using the equation $\upsilon_\theta = w \bullet r$, where υ_θ is the tangential velocity of the paddle at a particular radius, w is the angular (rotational) velocity of the paddle, and r is the distance from the center point of the paddle (radius). Conversion of the rotational velocity of the paddle to tangential velocities at the same radii, as examined in **Figure 6**, reveals that close to the bottom of the vessel (Z = –0.605) tangential velocities were approximately equal to those of the paddle (for the corresponding radius). For example, for the paddle at radius R = 0.344, tangential velocity = 5.236 × (0.344×0.051) = 0.092m/s = 0.47 relative tangential velocity, which is in close agreement with the corresponding simulated value for R = 0.344 at Z = –0.605. This graded increase in tangential velocity with increasing radius, equating to solid body rotation, was speculated by Bocanegra et al[11] and further confirms the simulated data. Maximal tangential velocities on this plane were in the region of 9 cm/s.

Axial Velocities 2.0 mm (Z = –0.066) Above the Paddle Wings

The changes in normalized axial velocities (relative to paddle tip), both measured and predicted, versus paddle radius are shown in **Figures 7A** and **7B**, respectively. Unlike in the tangential data discussed above, both positive (upward motion) and negative (downward motion) velocities occur. A 180° periodicity is exhibited by both experimental and simulated data. The velocity

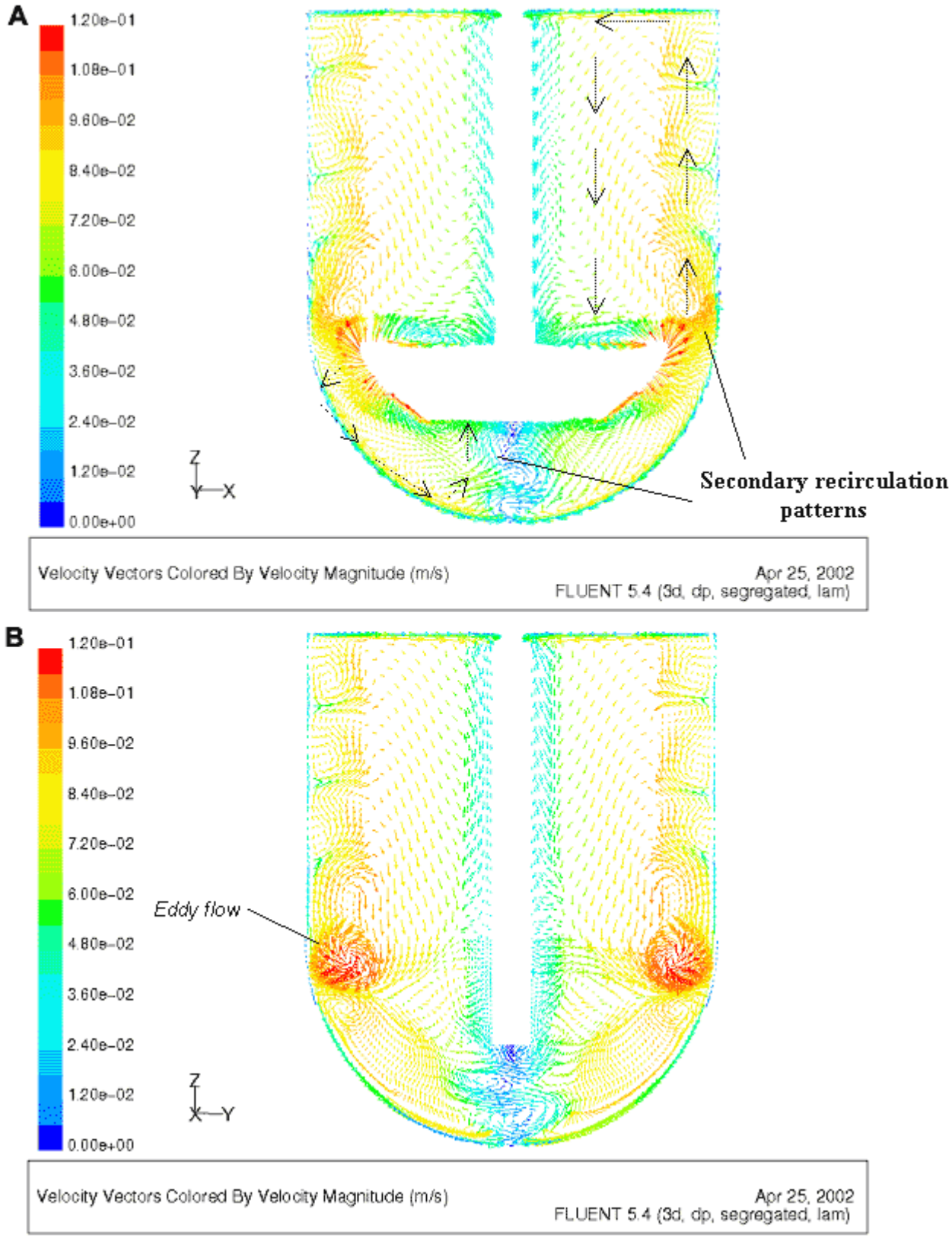

Figure 4. Simulated velocity vectors (A) on a midplane in line with the paddle wings, and (B) at 90° to the paddle wings in the USP dissolution apparatus at 50 rpm, colored by velocity magnitude (m/s) (only one sixth of cell values included for clarity).

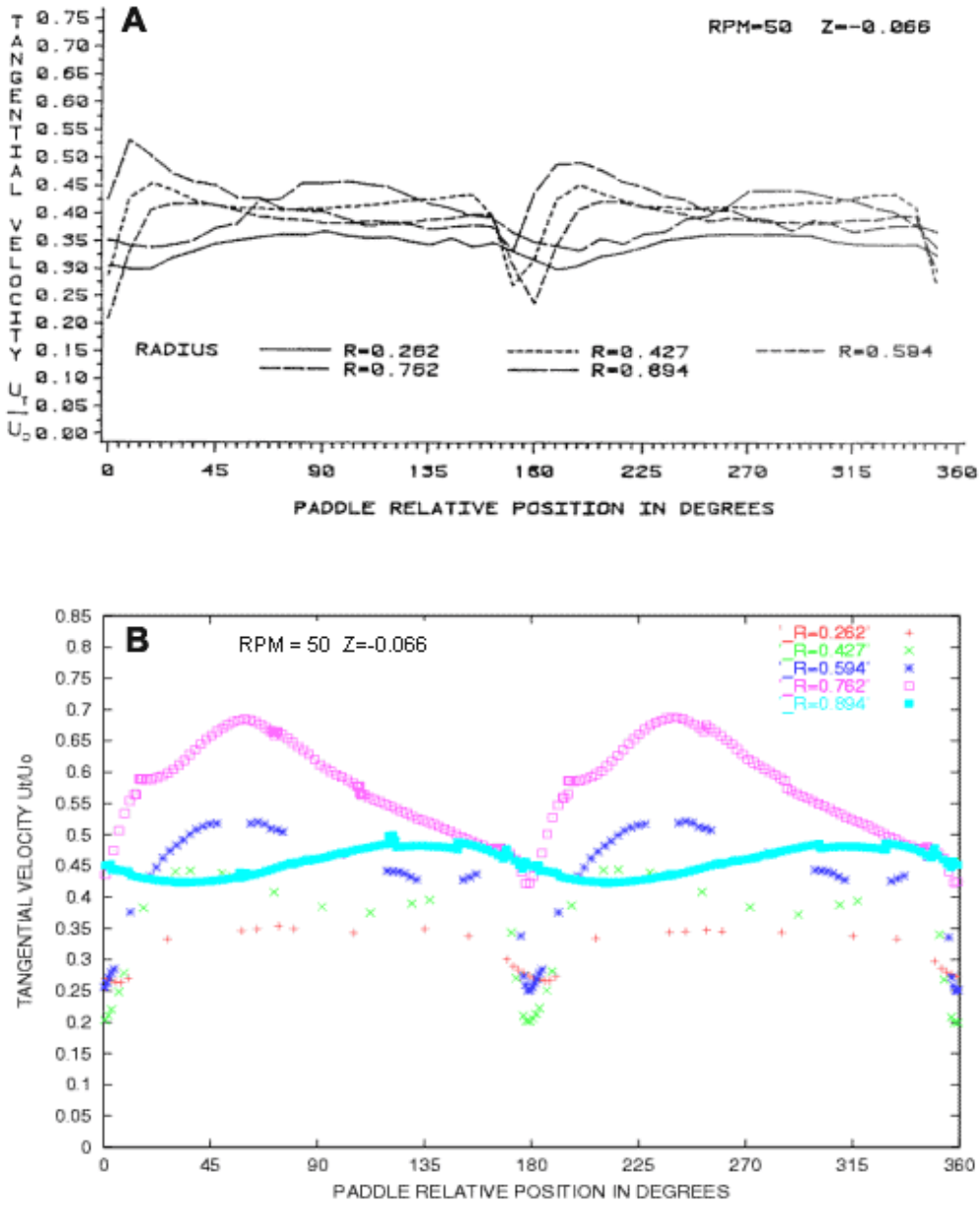

Figure 5. Comparison of CFD predicted and experimentally determined tangential velocities for 5 radii at a plane 2.0 mm above the top of paddle wings of the USP paddle dissolution apparatus (Z = –0.066). (A) Laser Doppler measured normalized tangential velocities, and (B) corresponding CFD predicted normalized tangential velocities. Figure 5A reprinted with permission from *Drug Development and Industrial Pharmacy.*[11] Copyright 1990, Marcel Dekker, Inc.

magnitudes are lower when compared to the tangential velocities (**Figure 5**).

The axial velocity changes, in magnitude as well as direction, with the relative position of the paddle and oscillates in the normalized velocity range from approximately 0.3 to approximately –0.25, which translates to actual velocities on this plane of 5.2 to –4.5 cm/s (**Figure 7**). Quantitatively, there is little difference between the 2 data sets for all radii examined, although the peaks for R = 0.762 are slightly more extreme for the simulated data and the troughs for the lowest radius are slightly lower for the simulated than the experimental measurements, as the paddle approaches 0° and 180° paddle relative position. An examination of velocities across this plane indicates the axial flow in the region immediately above the paddle

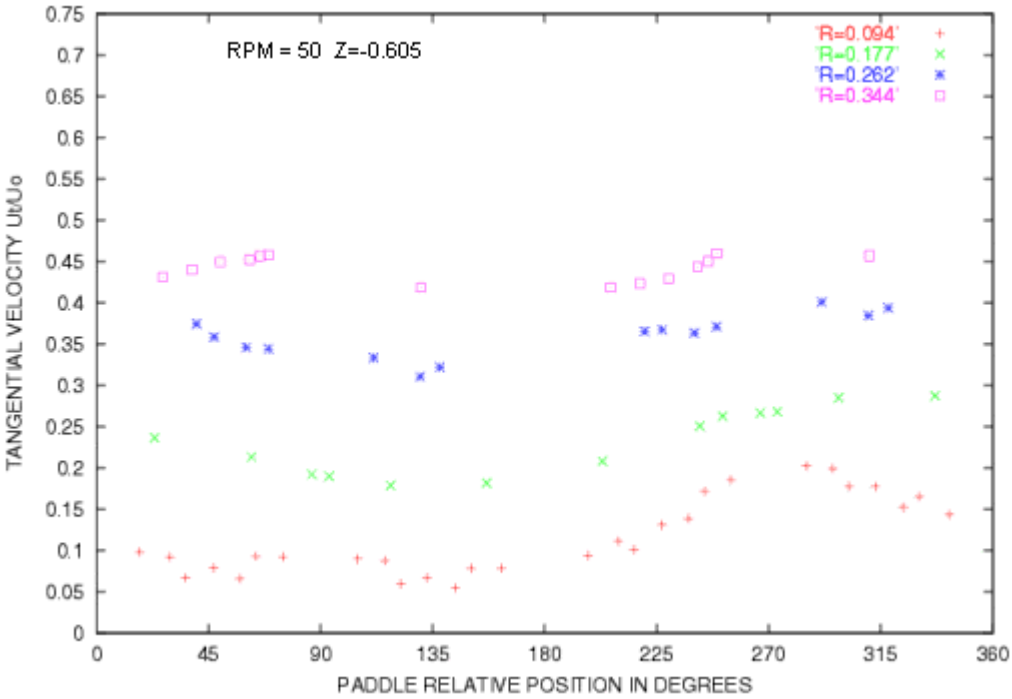

Figure 6. CFD predicted tangential velocities for 4 radii at a plane 5.3 mm from the base of the USP paddle dissolution apparatus (Z = –0.605).

to be quite complex. The volume immediately above the region swept out by the paddle wings is dominated by negative axial velocity (toward the base of the vessel), except for the region immediately in front of the paddle wings, which has a positive axial component. Outside of this area (between the paddle wings and wall) the fluid velocity has a high positive axial component.

Radial Velocities 16.2 mm (Z = –0.461) from the Base of the Vessel

The normalized (relative to paddle tip) predicted velocities below the paddle, at a plane 16.2 mm from the base of the vessel, are shown in **Figure 8**. Again, there is good qualitative agreement between simulated velocities and experimental data. Relative velocities are very low, indicating little radial fluid movement. All results fluctuate between –0.05 and 0.05, results not varying significantly for the 3 radii, for both the experimental and simulated velocities. A mild 180° periodicity was shown for the laser Doppler measurements and is also exhibited by the simulated data for the second and third radii, with a little fluctuation in the data of the lowest radius. Actual radial velocities on this plane ranged from –0.5 to 0.5 cm/s.

Quantitative Comparison of CFD Predictions and Laser Doppler Measurements of Bocanegra et al[11]

The CFD-generated velocities and the laser Doppler fluid velocity measurements of Bocanegra et al[11] are quantitatively compared (axial, tangential, and radial) at 3 different planes in the vessel in **Figure 9**. Error bars in the laser Doppler data were obtained from LM Bocanegra (written communication, June, 2002), as previously published data did not include an indication of the experimental error (Bocanegra et al[11]).

A linear regression analysis of laser Doppler measurements versus CFD-predicted velocities (at the same paddle relative position) for the above 3 data sets yielded correlation coefficients of 0.77, 0.76, and 0.93, respectively. More important, all CFD-predicted velocities were within the ±1 SD ranges of the laser Doppler experimental measurements. This close correlation between the 2 data sets gives us confidence in the validity of the CFD-generated velocities to effectively simulate hydrodynamics in the paddle dissolution apparatus.

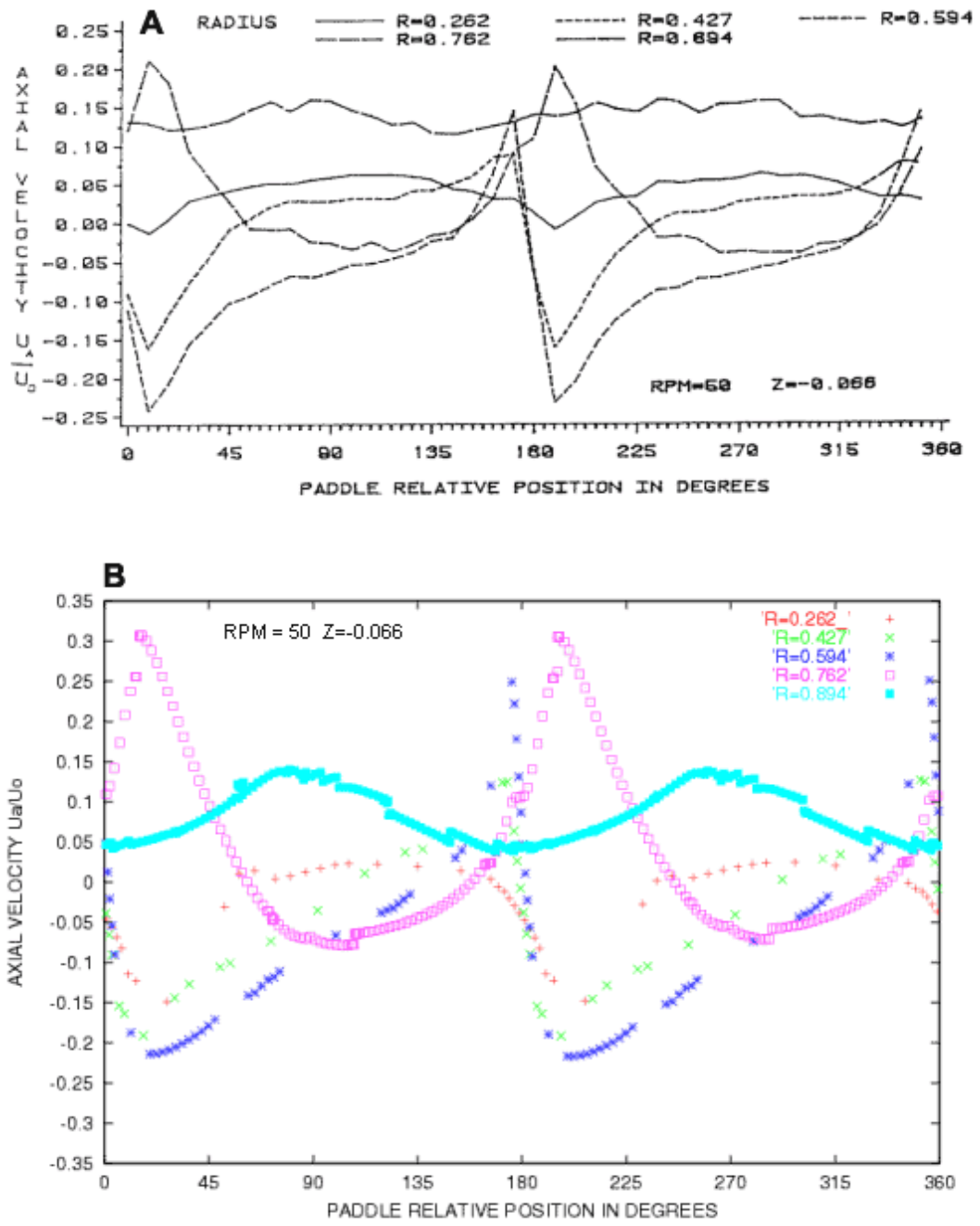

Figure 7. Comparison of CFD predicted and experimentally determined axial velocities for 5 radii at a plane 2.0 mm above the top of paddle wings (Z = –0.066). (A) Laser Doppler measured normalized axial velocities, and (B) corresponding CFD predicted normalized axial velocities. Figure 7A reprinted with permission from *Drug Development and Industrial Pharmacy.*[11] Copyright 1990, Marcel Dekker, Inc.

Comparison with Other Measurements of Fluid Flow in the Paddle Dissolution Apparatus

The hydrodynamics of the paddle dissolution test have recently been studied using an ultrasound pulse echo method.[12] Maximal tangential velocities were measured at a lateral distance of 26 mm from the center of the vessel for a series of heights within the vessel (S1-S4; see **Table 2**), and axial fluid velocities were measured at 2 radii from the top of the fluid into the bulk (O1 and O2; see **Table 2**). Fluid velocities were measured at different distances from the ultrasound probe to find

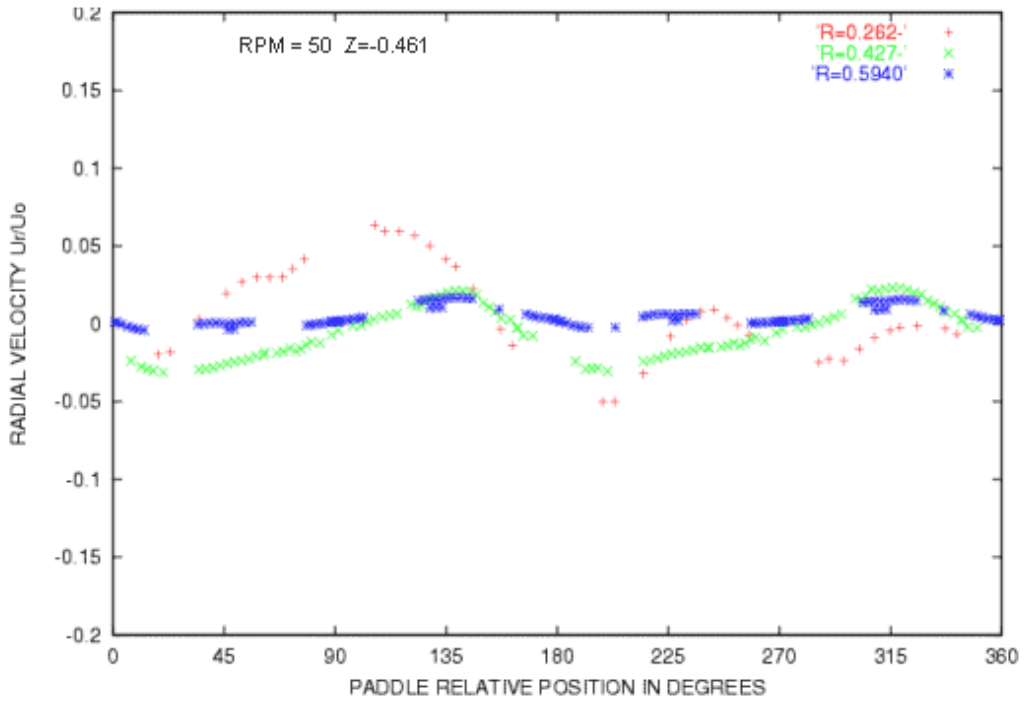

Figure 8. CFD predicted radial velocities for 3 radii at a plane 16.2 mm from the base of the USP paddle dissolution apparatus (Z = –0.461).

the maximum fluid velocity at a particular paddle rpm. Simulated velocities were determined for the corresponding positions in the CFD vessel. A comparison of the results at 50 rpm is shown in **Table 2**.

CFD-simulated results show good qualitative agreement with both the tangential and the axial measured velocities. This indicates the ability of the model to predict the secondary flow patterns studied by Diebold and Dressman.[12] However, although there was qualitative agreement, there was a quantitative discrepancy between the CFD-generated velocities and the ultrasound-measured velocities of fluid dynamics in the vessel. A possible reason for the discrepancy is that CFD is better able to predict bulk fluid flow at steady state, rather than predicting the behavior of fluids at local maxima such as those generated by the ultrasound method.

General Observations (Analysis of Fluid Dynamics on a Midplane Through the Vessel [50 rpm])

Since the CFD results of the structured grid approach were both qualitatively and quantitatively in close agreement with the laser Doppler measured values for a series of positions in the vessel, it was then possible to critically examine the fluid flow throughout the USP vessel in more detail. Simulated velocities on a plane aligned with the paddle wings were shown in **Figure 4A**.

Initial examination of **Figure 4** indicated that fluid velocities varied extensively with position throughout the vessel. The major component of fluid motion throughout the vessel was the tangential component. This is not surprising, as fluid flow is generated by the momentum transfer from the paddle via normal stresses and the paddle rotation is in the tangential direction. However, the paddle rotation will necessarily induce secondary flows in the axial and radial directions. The nature of such secondary flows in the USP paddle dissolution apparatus has been a matter of considerable speculation.[16-18] **Figure 4** provides an insight into the nature of the secondary flow in the axial direction at the midplane directly above and below the paddle. Bocanegra[17] noted that the axial secondary flow resulted in an oscillation of the flow and speculated that this observation was of potential importance to the sensitivity and reproducibility of resulting dissolution data. This observation was based on a number of laser Doppler measurements for specific single points in the vessel, the flow between these points being speculated flow. Examination of **Figure 4** substantiates the speculated fluid flow field of Bocanegra et al[11] for the midplane in

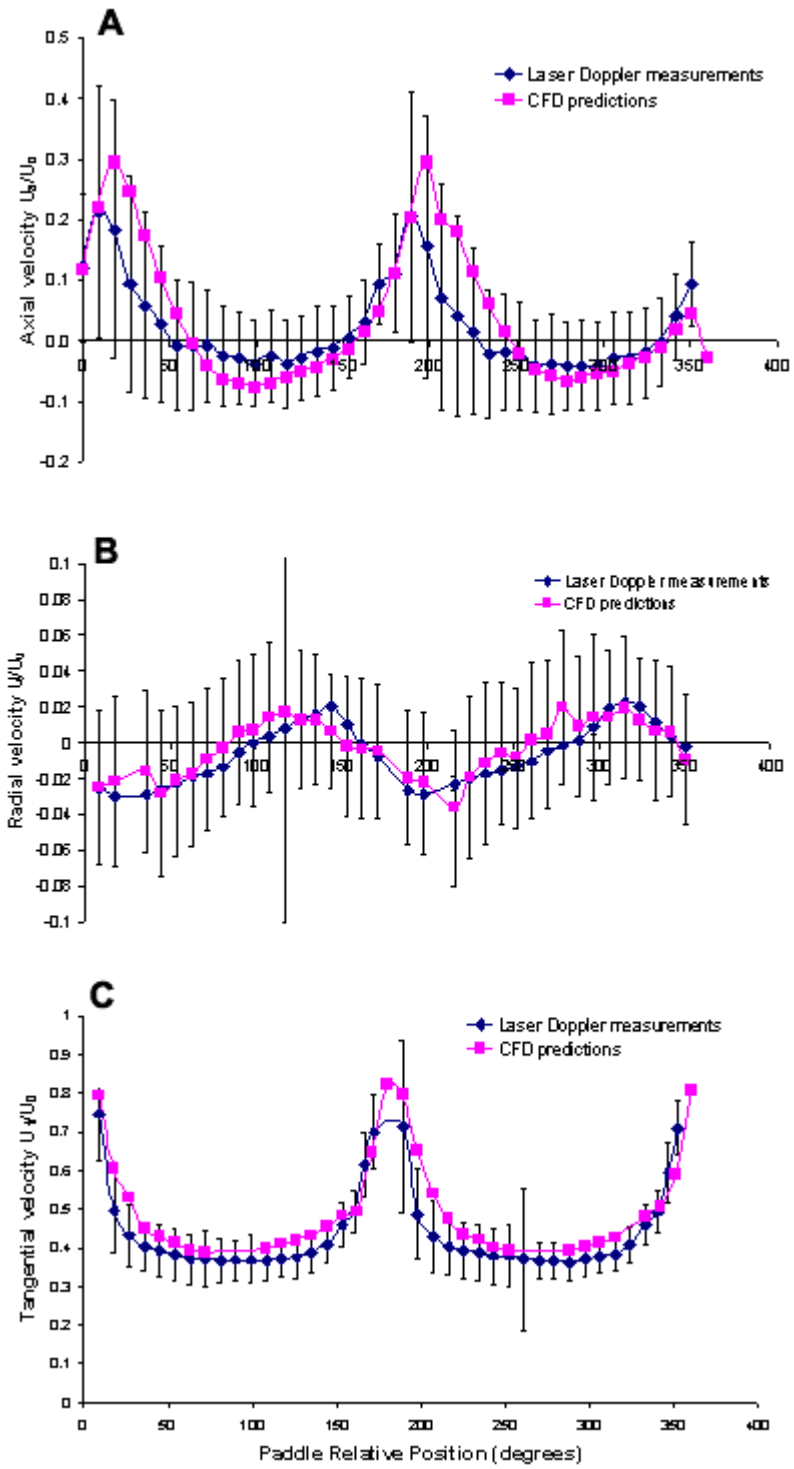

Figure 9. Comparison between laser Doppler fluid flow measurements[11] and CFD predictions of (A) axial velocities on a plane at Z = –0.066 for a radius R = 0.762; (B) radial velocities on a plane at Z = –0.461 for a radius R = 0.427; and (C) tangential velocities on a plane at Z = –0.197 for a radius R = 0.594. Error bars are the SDs of the laser Doppler measurements (LM Bocanegra et al, written communication, June, 2002).

Table 2. Comparison Between CFD Predicted and Ultrasound Measurements of Fluid Flow for Axial and Tangential Velocities in the Paddle Dissolution Apparatus for Various Positions in the Vessel, at 50 rpm*

Position Name	Velocity Type	Distance From Base (mm)	Distance From Center (mm)	Ultrasound Measurement (cm/s)	CFD Prediction (cm/s)
S1	Tangential, U_t	16	27.7	8.67	6.21
S2	Tangential, U_t	72	28.7	7.54	5.44
S3	Tangential, U_t	105	25.7	8.36	5.86
O1	Axial, U_a	29.1	25.5	1.09	3.09
O2	Axial, U_a	29.1	43.3	–1.41	–2.90

*Data from Diebold.[16] CFD indicates computational fluid dynamics.

the USP dissolution apparatus. Another interesting observation is a number of small regions of eddy flow immediately inside the vessel wall between the paddle and the surface of the liquid.

Above the paddle, the secondary axial flow is positive (upward) in the region near the vessel wall, while a negative (downward) axial flow is predicted in the region near the stirrer shaft, resulting in a secondary recirculation pattern. Examination of the radial flow from **Figure 8** indicates that there is little radial flow in the cylindrical volume of the vessel, apart from the region immediately above the paddle wings and at the top of the vessel volume, the points where recirculation is facilitated. The radial component of velocity is at its highest at the level of the paddle (radial pumping). It was speculated that the high radial component results in the formation of 2 distinct regions of mixing—that is, the cylindrical volume above the paddle (the sample acquisition region) and the hemispherical volume below the paddle (the primary drug dissolution region), as this radial component is later dissipated into an upward and a downward axial component at the vessel wall.[17]

Velocities below the paddle were more complicated than those above the paddle. Axial components were negative near the wall, gradually changing to positive toward the center. Radial velocities below the paddle have a high inward component in the region near the lower hemispherical wall and converge directly below the center of the paddle. Fluid velocities directly below the paddle at this convergence point appear to be involved in a local "vortex" flow, which will be examined in further detail later, as it is in this region that dissolution from a solid (or particulate) drug delivery system is likely to occur. Recalling that the axial velocity component varied significantly with regard to paddle relative position (**Figure 7B**), it is instructive to examine the velocities on another midplane, apart from that directly in line with the paddle.

Simulated velocities on a plane at 90° to the paddle wings are shown in **Figure 4B**. Fluid velocities in the region above and below the paddle at 90° to the paddle wings (**Figure 4B**) do not appear to quantitatively differ significantly from those where the paddle was in line with the plane (**Figure 4A**). However, this plane provides further insight into the nature of the mixing at the level of the paddle tip, between the 2 regions above and below this point. It appears that flow in this region is complicated by a region of eddy flow characterized by large changes in velocity components within a small region. This region of eddy flow results in a small area of local recirculation. As this is the main mixing route between the regions above and below this point, it appears that this region is a further hindrance to adequate mixing between these 2 areas. The region of complex flow toward the base of the vessel is also evident in this fluid plane. Again, small regions of eddy flow are predicted immediately inside the vessel wall, between the paddle and the surface of the liquid.

Velocity Contours Directly Below the Paddle

As drug dissolution will occur in the region directly below the paddle, fluid dynamics in this region are of particular interest. Contours of velocity magnitude on the midplane in line with the paddle wings, directly below the paddle, are shown in **Figure 10A**.

Although the fluid dynamics at the base of the USP dissolution apparatus are complex, it is evident that there is a large radial component toward the lower wall of the vessel. This region of high radial flow terminates directly below the center of the paddle at a region of low velocity. This domain of low velocity extends from

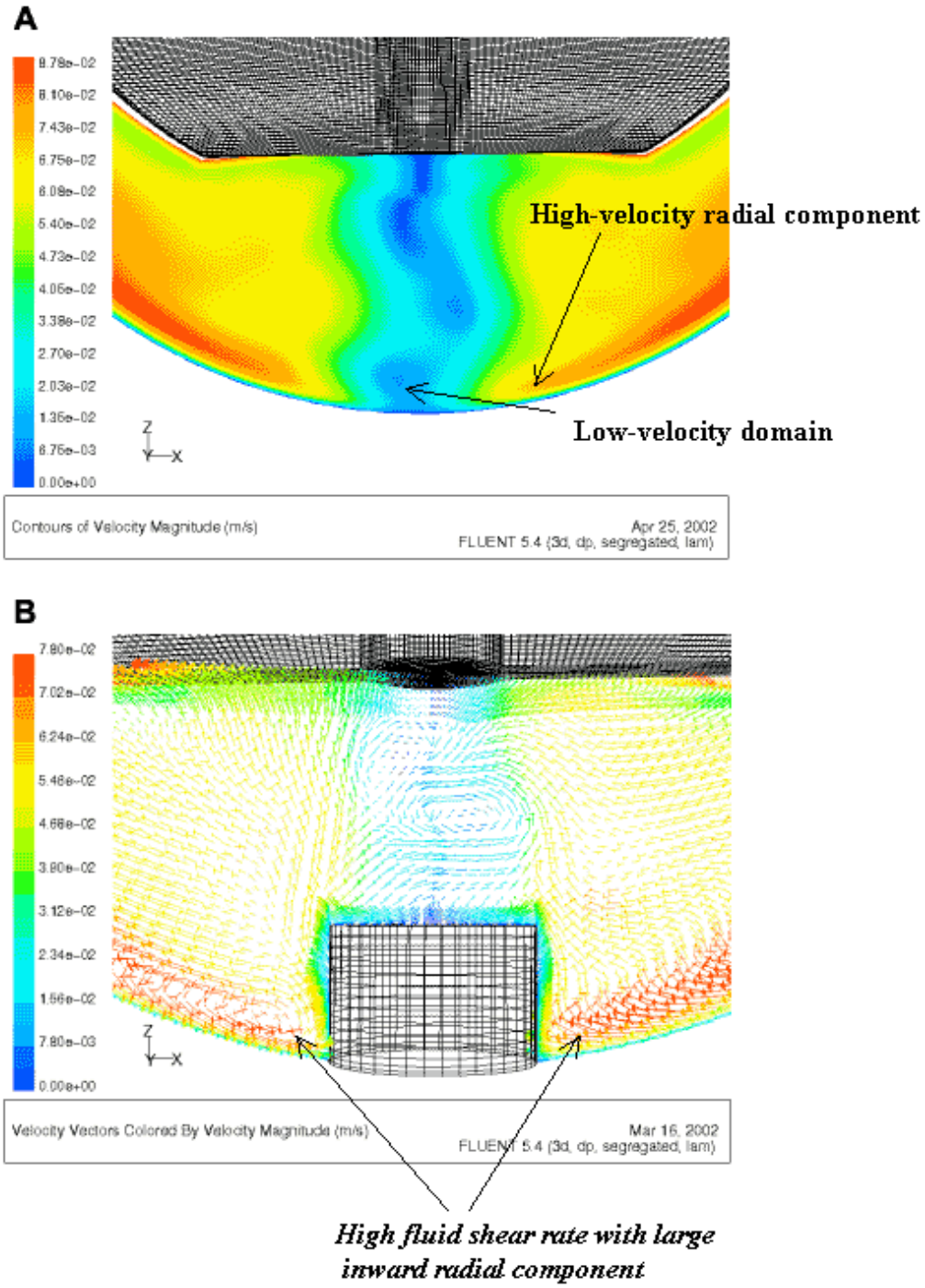

Figure 10. (A) Contours of velocity magnitude (m/s) on midplane in line with paddle wings directly below the paddle in the USP dissolution apparatus at 50 rpm, and (B) simulated velocity vectors (m/s) on a midplane in line with the paddle wings with a compact of 8.5 mm height situated at the base of the vessel. Not all grid points are included (for clarity).

the bottom of the vessel to the central lower part of the paddle. This low-velocity domain itself is surrounded by a region of higher velocity. At the base of the vessel (the point where the delivery system is likely to be situated) there is a 3- to 4-fold difference in fluid velocity rates between 2 regions approximately only 8 to 10 mm apart, as indicated in **Figure 10**. It is postulated that this large variation in fluid velocity over a very

short area directly below the paddle is likely to be one reason for the variable dissolution rates in the USP dissolution apparatus that have been previously reported.[5] It is possible that such erratic fluid dynamics would have a higher impact on a formulation that is situated within this region, compared to a buoyant system where random movements throughout the base of the vessel would diminish the effect of such hydrodynamics on the dissolution rates. At the base of this region of central low velocity exists a region of negligible fluid velocity. Qureshi and Shabnam[19] speculated that a region of "dead volume" is responsible for the appearance of a "cone" formation of particulate material during the dissolution test, owing to the decreased medium agitation and decreased surface area approaching the bottom of the hemispherical part of the vessel. The same authors suggested that the round bottom of a dissolution vessel, in combination with stirring devices (eg, paddle), results in varied flow dynamics within the vessel, which appears to be the cause of observed high variability in the testing.[20-22] The CFD-predicted fluid velocities above provide substantial support for such speculation.

Effect of the Presence of a Dosage Form on the Localized Hydrodynamics

A configuration was developed with a cylindrical tablet (13 mm × 8.5 mm) in place at the bottom of the USP vessel, and simulations at a paddle speed of 50 rpm were then generated. The effect of the presence of a cylindrical tablet at the base of the dissolution vessel on the fluid flow is shown in **Figure 10B**. This figure shows simulated velocities on a plane aligned with the paddle wings after inclusion of the tablet, with a high degree of grid refinement at the tablet surface interface. The presence of the tablet complicated the local fluid flow. Fluid shear rates varied depending on the tablet surface and the location on the surface, consistent with the variable dissolution observed.[5] A region of high fluid shear rate with a large inward radial component is clearly evident toward the base of the compact. This region of high fluid shear rate is consistent with what we have previously reported[5] about the preferential erosion toward the base of compacts following dissolution in the USP paddle dissolution apparatus. **Figure 11** contains a photograph showing the variable erosion of a cylindrical tablet before and after dissolution for 1 hour at 50 rpm. As the compact dissolves, a groove appears on the curved surface of the compact toward the base, where dissolution has occurred at a faster rate than it has higher up.

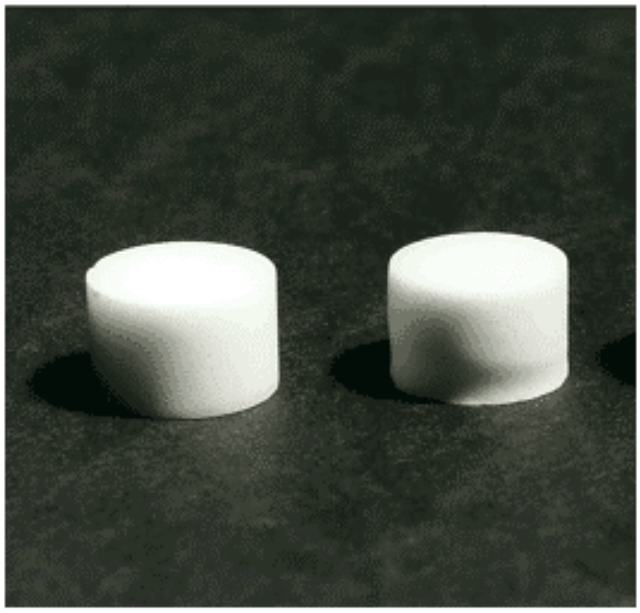

Figure 11. Photograph of benzoic acid compact before dissolution and after dissolution for 1 hour, at 50 rpm.

CONCLUSION

The CFD-generated fluid velocities were in close agreement with the laser Doppler measurements. Analysis of the behavior of the fluid on vertical midplanes through the vessel provided further insight into the flow behaviors that lead to fluid recirculation throughout the vessel. These secondary flow patterns were in agreement with those previously speculated.[11,18] The predominant component of velocity throughout the vessel was the tangential component, although the axial and radial components were quite high in the region of the paddle impeller. Velocity vectors at 90° to the paddle impeller revealed a region of high eddy flow at the same horizontal level as the paddle tip, which was speculated to be a possible hindrance to mixing between the 2 regions. Examination of fluid flow behavior below the level of the paddle revealed a region with a high inward radial velocity component, immediately inside the wall of the hemispherical base, from a region below the impeller to a region near the base of the hemisphere. However, centrally, at the base of the hemisphere, a region of low–fluid velocity magnitude was evident. Directly outside this region, the magnitude of fluid velocity was considerably higher (3 to 4 times change in velocity over a distance of approximately 8-10 mm). In fact, the fluid at the base of the vessel has negligible fluid velocity toward the center of the base for a region of diameter approximately 10 to 15 mm. This region extended upward toward the bottom of the paddle.

This approach, using CFD as a tool that allows the hydrodynamics at any point in the dissolution vessel to be predicted, has the potential to explain variability in dissolution results obtained with the USP apparatus 2 and also to aid in the determination of optimal dissolution conditions for IVIVC.

REFERENCES

1. Levy G. Effect of certain tablet formulation factors on dissolution rate of the active ingredient I. J Pharm Sci. 1963;52:1039-1046.

2. Kamba M, Seta Y, Kusai A, Nishimura K. Comparison of the mechanical destructive force in the small intestine of dog and human. Int J Pharm. 2002;237(1-2):139-149.

3. Rohrs BR, Skoug JW, Halstead GW. Dissolution assay development for in vitro-in vivo correlations. In: Young D, Devane JG, Butler JB, eds. In Vitro-In Vivo Correlations. New York, NY: Plenum Press; 1997:17-30.

4. USP 26, The United Stated Pharmacopeia. Rockville, MD: United States Pharmacopeial Convention Inc; 2003:2155-2156.

5. Healy AM, McCarthy LG, Gallagher KM, Corrigan OI. Sensitivity of dissolution rate to location in the paddle dissolution apparatus. J Pharm Pharmacol. 2002;54:441-444.

6. Levy G. Effect of dissolution rate on absorption, metabolism and pharmacologic activity of drugs. J Mond Pharm. 1967;3:237-254.

7. Stricker H. In vitro studies on the dissolution and absorption behaviour of orally administered drugs and the connection to their bioavailability. In: Deasy PB, Timoney RF, eds. The Quality Control of Medicines. Amsterdam, The Netherlands: Elsevier Scientific Publishing Company; 1976:253-271.

8. Weiss A, Pitman ER, Graham EC. Aspirin and gastric bleeding: gastroscopic observations, with review of literature. Am J Med. 1961;31:266-278.

9. Levy G, Leonards JR, Procknal JA. Development of in vitro dissolution tests which correlate quantitatively with dissolution rate-limited drug absorption in man. J Pharm Sci. 1965;54:1719-1722.

10. Scholz A, Abrahamsson B, Diebold SM, Kostewicz E, Polentarutti BI, Ungell A-L, Dressman JB. Influence of hydrodynamics and particle size on the absorption of felodipine in labradors. Pharm Res. 2002;19:42-46.

11. Bocanegra LM, Morris GJ, Jurewicz JT, Mauger JW. Fluid and particle laser Doppler velocity measurements and mass transfer predictions for the USP paddle method dissolution apparatus. Drug Dev Ind Pharm. 1990;16:1441-1464.

12. Diebold SM, Dressman JB. Hydrodynamik kompendialer Lösungsgeschwindigkeits-Testapparaturen. Pharm Ind. 2001;63:94-104.

13. Fluent5 User's Guide. Vols 1-4. Canterra Resource Park, NH: Fluent Incorporated; 1998.

14. Munson BR, Young DF, Okiishi TH. Fundamentals of Fluid Mechanics. New York, NY: John Wiley & Sons Inc; 1998:309-365.

15. Visawanth DS, Natarajan G. Data Book on the Viscosity of Liquids. New York, NY: Hemisphere Publishing Corporation; 1989:41-45, 714-715.

16. Diebold SM. Hydrodynamik and Lösungsgeschwindigkeit [dissertation]. Frankfurt, Germany: Wolfgang Goethe-Universität; 2000.

17. Bocanegra LM. A Two Phase Flow Experimental Study of the United States Pharmacopeia Paddle Method Dissolution Test Apparatus [dissertation]. Morgantown, WV: West Virginia University; 1988.

18. Beckett AN, Quach TT, Kurs GS. Improved hydrodynamics for USP apparatus 2. Dissolut Technol. 1996;3:7-10.

19. Qureshi SA, Shabnam J. Cause of high variability in drug dissolution testing and its impact on setting tolerances. Eur J Pharm Sci. 2001;12:271-276.

20. Cox DC, Wells CE, Furnam WB, Savage TS, King AC. Systematic error associated with apparatus 2 of the USP dissolution test, II: effects of deviations in vessel curvature from that of a sphere. J Pharm Sci. 1982;71:395-399.

21. Achanta AS, Gray VA, Cecil TL, Grady LT. Evaluation of the performance of prednisone and salicylic acid calibrators. Drug Dev Ind Pharm. 1995;21:1171-1182.

22. Qureshi SA, McGilveray IJ. Typical variability in drug dissolution testing: study with USP and FDA calibrator tablets and a marketed drug (glibenclamide) product. Eur J Pharm Sci. 1999;7:249-258.